BIOCHEMISTRY
including biophysical chemistry & molecular biology

Article

pubs.acs.org/biochemistry

Mutational and Computational Evidence That a Nickel-Transfer Tunnel in UreD Is Used for Activation of *Klebsiella aerogenes* Urease

Mark A. Farrugia,[†] Beibei Wang,[†] Michael Feig,[†,‡] and Robert P. Hausinger*[,†,§]

[†]Department of Biochemistry and Molecular Biology, [‡]Department of Chemistry, and [§]Department of Microbiology and Molecular Genetics, Michigan State University, East Lansing, Michigan 48824, United States

Supporting Information

ABSTRACT: Nickel-containing urease from *Klebsiella aerogenes* requires four accessory proteins for proper active site metalation. The metallochaperone UreE delivers nickel to UreG, a GTPase that forms a UreD/UreF/UreG complex, which binds to urease apoprotein via UreD. Prior *in silico* analysis of the homologous, structurally characterized UreH/UreF/UreG complex from *Helicobacter pylori* identified a water tunnel originating at a likely nickel-binding motif in UreG, passing through UreF, and exiting UreH, suggestive of a role for the channel in providing the metal to urease apoprotein for its activation; however, no experimental support was reported for the significance of this tunnel. Here, specific variants were designed to disrupt a comparable 34.6 Å predicted internal tunnel, alternative channels, and surface sites for UreD. Cells producing a set of tunnel-disrupting variants of UreD exhibited greatly reduced urease specific activities, whereas other mutants had no appreciable effect on activity. Affinity pull-down studies of cell-free extracts from tunnel-disrupting mutant cultures showed no loss of UreD interactions with urease or UreF/UreG. The nickel contents of urease samples enriched from activity-deficient cultures were decreased, while zinc and iron incorporation increased. Molecular dynamics simulations revealed size restrictions in the internal channels of the UreD variants. These findings support the role of a molecular tunnel in UreD as a direct facilitator of nickel transfer into urease, illustrating a new paradigm in active site metallocenter assembly.

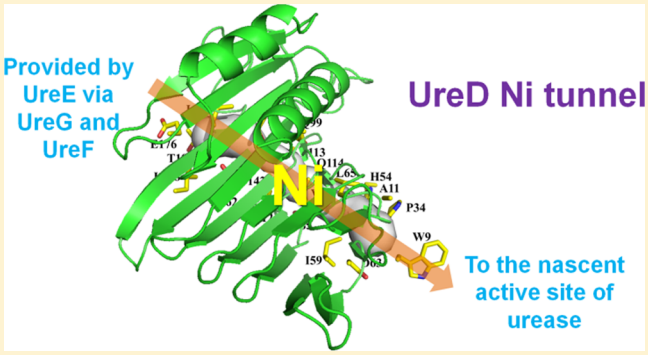

Urease catalyzes the hydrolysis of urea into ammonia and carbamate, with the latter compound spontaneously decomposing into a second molecule of ammonia and bicarbonate.[1,2] The enzyme is found in plants[3] as well as some bacteria, archaea, algae, and fungi.[4] Most of our knowledge about the formation of the nickel active site[5] comes from studies of the urease activation machinery of *Klebsiella aerogenes* and *Helicobacter pylori*, as detailed below.

The urease gene cluster from *K. aerogenes* (*ureDABCEFG*)[6] encodes three enzyme subunits (*Ka*UreA, *Ka*UreB, and *Ka*UreC) and four accessory proteins (*Ka*UreD, *Ka*UreE, *Ka*UreF, and *Ka*UreG). The subunits assemble into $(KaUreABC)_3$,[7] with the dinuclear active site located in UreC. *Ka*UreD, when fused to the maltose-binding protein (MBP−UreD), is soluble and binds over 2 equiv of nickel.[8] *Ka*UreF alone is insoluble.[9] *Ka*UreG, which exists as a soluble monomer that binds 1 equiv of nickel or zinc with similar affinities,[10,11] acts as a GTPase during urease maturation, although the precise role of GTP hydrolysis in this process remains unclear. *Ka*UreG residues associated with a highly conserved Cys-X-His motif are hypothesized to function as the metal binding site, but substitution of one or both of these residues does not abolish metal binding.[11] The crystal structure of *Ka*UreE is known,[12] and the dimeric nickel-binding protein is proposed to deliver nickel for urease activation.[13] Attempts to activate *K. aerogenes* urease *in vivo* in the absence of any accessory protein result in the production of inactive enzyme lacking nickel.[6,14] The purified apoprotein can be partially activated *in vitro*,[15,16] and the activation competence is enhanced for urease apoprotein in complex with UreD,[16−19] UreD/UreF,[18−20] and UreD/UreF/UreG.[21] UreD/UreF/UreG is formed *in vivo*, though direct studies of this complex were limited due to its low solubility.[10] In contrast, a soluble complex is formed with MBP−UreD, producing $(MBP−UreD/UreF/UreG)_2$ that dissociates to the monomer of heterotrimers when bound to urease.[22]

The *H. pylori* urease gene cluster (*ureABIEFGH*)[23] is similar to that from *K. aerogenes*, but the encoded proteins exhibit a few important distinctions. The enzyme contains two subunits (*Hp*UreA is homologous to a *Ka*UreA−UreB fusion, while *Hp*UreB is homologous to *Ka*UreC) that assemble into $((HpUreAB)_3)_4$.[24] *Hp*UreF was structurally characterized,[25] and isothermal titration calorimetry demonstrates that it binds nickel,[26] although the functional relevance of metal binding was not tested. *Hp*UreG is a monomer in the absence of metal, binds zinc with high affinity leading to dimerization, and binds

Received: August 21, 2015
Revised: September 24, 2015
Published: September 24, 2015

DOI: 10.1021/acs.biochem.5b00942
Biochemistry 2015, 54, 6392−6401

nickel with low affinity without facilitating dimerization of the protein.[27] The structure of dimeric *Hp*UreE[28] closely resembles that of *Ka*UreE, and it forms a complex with *Hp*UreG.[29] Finally, *H. pylori* encodes a proton-gated urea permease (UreI).[30] Of great significance to urease activation, the crystal structure of $(HpUreH/UreF/UreG)_2$ is known[31] (*Hp*UreH is homologous to *Ka*UreD), although the interaction surface of this complex with urease has not been determined.

While the importance of the accessory proteins to urease maturation is clear, the exact mechanism of this process is still unknown with two main hypotheses posited. One proposal invokes a "hand-off" mechanism with cytosolic nickel binding to the UreE metallochaperone, which then passes it to surface-exposed residues of UreG,[11] possibly UreF, then UreD, and finally into the nascent active site of *K. aerogenes* urease apoprotein, all within the urease/UreD/UreF/UreG complex.[8,11] The second hypothesis involves the initial delivery of nickel from UreE to UreG, followed by the use of a buried channel connecting the proposed nickel-binding site of UreG, through UreF and UreH, directly into the nascent active site of *H. pylori* urease.[26] Thus far, no experimental data have been reported to support the function of this tunnel in nickel delivery for urease maturation.

Here, the function of *Ka*UreD in urease activation was examined. Targeted *Ka*UreD side chain substitutions were created, and the biological effects of these changes were characterized. The results support the existence of a tunnel in *Ka*UreD that is used for nickel delivery to urease, with additional evidence derived from comparisons of the molecular dynamics (MD) of the internal channels in wild-type (WT) and variant proteins. This work provides insights into how UreD functions in urease activation and illustrates how a metal transfer tunnel can be utilized for metallocenter assembly.

MATERIALS AND METHODS

Plasmid Construction. To characterize the effects of point substitutions on the function of *Ka*UreD *in vivo*, three types of plasmids were constructed, that is, pMF001L*, pKK17D*, and pKKD*G, where * indicates the mutant versions.

An *Eco*RI/*Hin*dIII fragment of pEC002[8] containing *ureD* was inserted into similarly digested pUC8 to yield plasmid pMF001. This plasmid cannot be used to directly overproduce UreD because it was found to lack a critical upstream region needed for overexpression, so an *Eco*RI/*Age*I fragment of pKK17[13] (containing *ureD* and a 197-bp 5′ untranslated region) was substituted into similarly digested pMF001 to yield pMF001L. The accessory gene within pMF001L was mutated by polymerase chain reaction with overlapping oligonucleotides (Integrated DNA Technologies, Coralville, IA) containing the proper base-pair substitution(s) and amplified with *Pfu*Turbo polymerase (Agilent Technologies). The resulting pMF001L* products were digested with *Dpn*I and transformed into *Escherichia coli* MAX Efficiency DH5α cells (Life Technologies). Mutagenesis was confirmed by sequencing (Davis Sequencing, Davis, CA, or Michigan State University Genomics Core, East Lansing, MI).

To study the effects of *ureD* mutations within the intact urease gene cluster, the pMF001L* versions were digested and the desired *ureD*-containing fragments were isolated as described above. These fragments were ligated into similarly treated pKK17 to yield the analogous versions of plasmid pKK17D*. These plasmids were also sequenced to ensure that the proper insertions were present.

To examine the effects of substitutions in *Ka*UreD on protein−protein interactions, WT and mutant *Eco*RI/*Age*I *ureD* fragments from pMF001L* were ligated into the similarly digested and isolated backbone of pKKG.[11] The resulting pKKD*G plasmids contain the *ureD* versions within the context of $ureDABCEFG_{Str}$, where *Ka*UreG has been modified with a C-terminal *Strep*-II tag ($KaUreG_{Str}$). The resulting plasmid validities were confirmed by sequencing. A summary of all plasmids used in these studies can be viewed in Table 1.

UreD Homology Model Generation and Refinement, Conservation Mapping, Water Tunnel Prediction, and Molecular Dynamics. A homology model was prepared by using the Protein Homology/analogY Recognition Engine (Phyre2, version 2.0) server[32] and the crystal structure of *Hp*UreH from the *Hp*UreH/UreF/UreG complex (PDB code 4HI0)[31] as a template. A PSI-BLAST analysis[33] was performed for *Hp*UreH, sequences with more than 15% and less than 90% identity were identified, the top 30 were selected along with *Ka*UreD for multiple sequence alignment,[34] and the residue conservation scores were mapped onto the *Ka*UreD homology model using the ConSurf server.[35] Initial homology models were refined with an MD-based protocol developed by us and validated in recent rounds of CASP (Critical Assessment of protein Structure Prediction).[36] Briefly, ten 40 ns simulations with weak restraints on all Cα atoms were performed starting with the homology model and using a force constant of 0.5 kcal mol^{-1} $Å^{-2}$. A subset of snapshots was selected from the generated sampling based on scoring. Subsequent averaging led to the refined structure that was used in subsequent simulations.

To determine the effects of point substitutions on the hypothetical water tunnels within *Ka*UreD, a series of MD simulations were carried out for WT *Ka*UreD and ten *Ka*UreD variants (E176A, E176Q, D63A, D63Q, D142A, S85K, L65I, L65W, T128E, and T196K) as well as the *Hp*UreH/UreF/UreG complex. All of the variant structures were generated in VMD.[37] The molecules were solvated with cubic boxes that were large enough to keep at least a 9 Å margin from any protein atom to the edge of the box. Cl^- and Na^+ were added by replacing water molecules randomly, yielding neutralized systems and a 20 mM NaCl solution, consistent with the concentration of the cytosol.[38] The final systems contained about 27 000 atoms (*Ka*UreD alone) or 152 000 atoms (*Hp*UreH/UreF/UreG complex).

All of the simulations were performed with NAMD 2.9[39] using the CHARMM36 force field.[40,41] The particle-mesh Ewald method[42] and the SETTLE algorithm[43] were used to calculate the electrostatic interactions and to constrain heavy atom-hydrogen bonds, respectively. The nonbonded interactions were truncated at 10 Å with a switching function at 8.5 Å. The systems were maintained at constant temperature and pressure of 298 K and 1 bar, respectively, using a Langevin-type thermostat and barostat.[44,45] The complete systems were first minimized over 5000 steps and equilibrated over 200 ps with the protein fixed. The temperature was gradually increased from 5 to 300 K with a step of 50 K over 400 ps without any restraints. Simulations were run with a weak harmonic restraint on Cα atoms using a force constant of 10 kcal mol^{-1} $Å^{-2}$ and reduced to zero in steps of 2 kcal mol^{-1} $Å^{-2}$ over 500 ps. Subsequent 3 × 50 ns of MD simulations were accumulated without any restraints for each system.

MOLE[46] is a powerful tool to explore molecular channels, tunnels, and pores based on Voroni diagrams where the optimal

DOI: 10.1021/acs.biochem.5b00942
Biochemistry 2015, 54, 6392−6401

Table 1. Plasmids Used in This Study

plasmid	description	source
pUC8	high-copy number plasmid containing the pBR322 origin of replication and the multiple cloning site of M13mp7 and conferring Amp^R. Gene expression is driven by an upstream *lac* promoter.	65
pKK17	*Eco*RI–*Hin*dIII fragment of *K. aerogenes ureDABCEFG* ligated into similarly digested pKK223-3 containing the pBR322 origin of replication, an upstream *tac* promoter, and downstream *rrnB* ribosomal terminator sequence and conferring Amp^R	13,66
pKK17D*, -V37L, -Y42D, -E46A, -E46Q, -C48A, -H49A, -H54A, -I59Y, -D63A, -D63Q, -L65I, -L65W, -S85K, -K86A, -Y88V, -Y88F, -R89A, -W111Y, -T128E, -D142A, -R148M, -E153A, -E153Q, -R163A, -E165A, -D169A, -E176A, -E176Q, -T196 K, -R211A	*Eco*RI–*Age*I *ureD* mutant fragments from pMF001L* ligated into similarly digested pKK17	this study
pKKG	*Pst*I–*Kpn*I $ureG_{Str}$ fragment ligated into similarly digested pKK17 resulting in replacement of UreG with one containing a C-terminal *Strep*-II tag ($ureDABCEFG_{Str}$)	11
pKKD*G, -D63A, -D63Q, -S85K, -D142A, -E176A, -E176Q, -R211A	*Eco*RI–*Age*I *ureD* mutant fragments from pMF001L* ligated into similarly digested pKKG	this study
pEC002	pMal-c2X derived vector using the pBR322 origin of replication and conferring Amp^R for the cytosolic overproduction of maltose binding protein fused at the N-terminus of UreD. Gene expression is governed by an upstream *tac* promoter and a downstream *rrnB* ribosomal terminator sequence.	8
pMF001	*Eco*RI–*Hin*dIII *ureD* fragment from pEC002 ligated into similarly digested pUC8	this study
pMF001L	*Eco*RI–*Age*I *5′UTR-ureD* fragment from pKK17 ligated into similarly digested pMF001	this study

path is searched for by the Dijkstra algorithm from a given starting point to the molecular surface. MOLE 2.0 was used to predict water tunnels within the refined *Ka*UreD homology model and the *Hp*UreH/UreF/UreG structure with a minimum radius of 1.2 Å. The electrostatics calculations were performed in APBS[47] at pH 7.0 with default parameters. RMSDs were calculated for all heavy atoms except the N- and C-terminal loop (residues 1−10 and 255−270) and the fixed radius clustering analysis was carried out in MMTSB[48] with an RMSD radius cutoff of 2.5 Å. Clusters were determined based on mutual, pairwise RMSD that results in overall similar structures to be grouped together. The conformation in a given cluster that was closest to the cluster center was used to represent the conformation of all the structures in this cluster. All the figures were generated in PyMOL.[49]

Urease Activity Assays. Enzyme activity was measured by quantifying ammonia release from urea using methods described by Weatherburn.[50] The release of ammonia over time was monitored by the formation of indophenol on the basis of its absorption of light at 625 nm. One unit of urease activity is defined as the amount of enzyme required to hydrolyze 1 μmol of urea per minute at 37 °C. The standard assay buffer was 50 mM 4-(2-hydroxyethyl)-1-piperazineethanesulfonic acid (HEPES), pH 7.8, with 50 mM urea.

***In Vivo* Activation of Urease by Variant *Ka*UreDs.** *E. coli* BL21(DE3) competent cells were transformed with pKK17D* or pKKD*G and plated on lysogeny broth (LB) agar plates supplemented with 300 μg/mL ampicillin. A single transformant colony was used to inoculate 2 mL of LB medium that was supplemented with 100 μg/mL ampicillin and cultured overnight. Aliquots (150 μL) of these overnight cultures were used to inoculate 15 mL of LB supplemented with 1 mM $NiCl_2$ and 100 μg/mL ampicillin in 50 mL flasks, which were shaken at 200 rpm at 37 °C until they reached an optical density at 600 nm (OD_{600}) of 0.5, induced with 0.1 mM isopropyl β-D-1-thiogalactopyranoside (IPTG), and grown overnight at 37 °C. Urease apoprotein was prepared in a similar manner, but with the culture medium lacking supplemental nickel. Cells were harvested by centrifugation and resuspended in 2.5 mL of 100 mM HEPES, pH 7.8, per gram of wet cell paste. Cells were lysed by sonication while placed in an ethanol ice bath by using a Branson 450 sonifier with three 2 min cycles at 4 W output power, 50% duty cycle, and 1 min of temperature recovery between cycles. Cell lysates were clarified by centrifugation at 100 000*g* at 4 °C for 1 h. The soluble cell-free extracts were diluted 100-fold into 100 mM HEPES, pH 7.8, buffer for urease activity assays. Overproduction of urease subunits was confirmed by sodium dodecyl sulfate−polyacrylamide gel electrophoresis (SDS-PAGE).

Protein Purification. To determine the metal contents of urease produced by cultures with a functionally deficient *Ka*UreD, *E. coli* BL21(DE3) cells were transformed with pKKD*G constructs of interest. A single transformant colony was inoculated into 5 mL of LB supplemented with 100 μg/mL ampicillin and cultured overnight. For each UreD variant used, 1 L of LB supplemented with 1 mM $NiCl_2$ and 100 μg/mL of ampicillin was inoculated with 1 mL of overnight culture, and bacteria were grown until they reached an OD_{600} of ∼0.6. These cultures were induced with 0.1 mM IPTG and grown overnight with shaking at 37 °C. Cells were harvested by centrifugation and resuspended in 2.5 volumes of buffer containing 50 mM Tris-base, pH 7.4, containing 1 mM EDTA, and 1 mM β-mercaptoethanol (TEB) that was

DOI: 10.1021/acs.biochem.5b00942
Biochemistry 2015, 54, 6392−6401

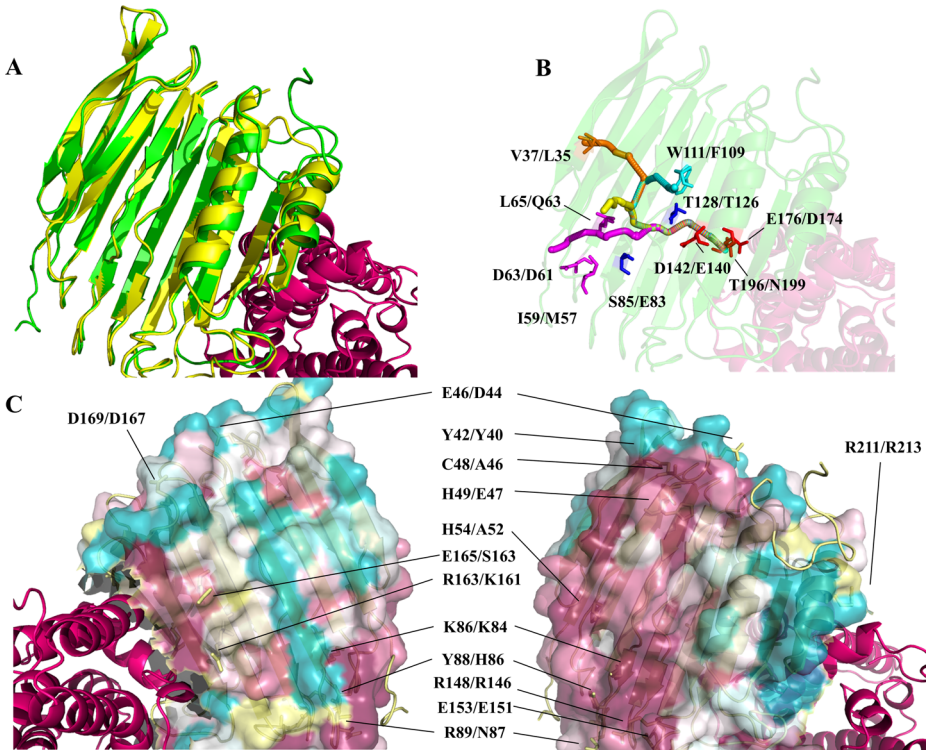

Figure 1. Homology-model guided mutagenesis of *Ka*UreD. (A) *Ka*UreD model (green) aligned to *Hp*UreH (yellow) from the *Hp*UreH/UreF/UreG crystal structure. *Hp*UreF (magenta) is shown to define the *Hp*UreH/UreF interaction site. (B) Tunnels predicted for the *Ka*UreD model. The color of residues corresponds to the associated exit (tunnel 1 = magenta, 2 = yellow, 3 = orange, and 4 = teal). Blue residues are positioned at the branch point shared by all tunnels, while red residues are located at the entrance point of the tunnel. (C) Two views (180° *y*-axis rotation) of the *Ka*UreD model colored by conservation score and depicted in surface representation. Dark blue, white, and dark magenta denote low, average, and high conservation. Surface and buried residues not associated with predicted water tunnels are labeled. Residues are noted with *K. aerogenes/H. pylori* numbering.

supplemented with 0.1 mM PMSF. Cells were lysed by sonication while immersed in an ethanol ice bath using a Branson 450 sonifier with three 2 min cycles at 4 W output power and 50% duty cycle including 1 min of temperature recovery between cycles. Soluble cell-free extracts were separated from unbroken cells and debris by centrifugation at 100 000*g* for 1 h at 4 °C. Supernatants were diluted 1:1 in TEB buffer before being applied to a 90 mL Macro-Prep DEAE Support (Bio-Rad) column pre-equilibrated in TEB buffer. The samples were washed with one volume of TEB buffer and eluted by using a 0 to 1 M NaCl gradient in TEB buffer. Fractions containing urease were pooled, dialyzed into TEB buffer containing 25 mM NaCl, and concentrated to 1 mL by using an Amicon Ultra-15 10K centrifugal filter (Millipore). Each concentrate was injected directly onto 100 mL columns containing either Superdex 200 (General Electric) or Sephacryl 300 HR (Sigma) resin pre-equilibrated in TEB buffer containing 25 mM NaCl. Proteins were eluted by using the same buffer, and the fractions containing urease were pooled and concentrated to 2.5 mL. The pooled samples were analyzed for their purity by SDS-PAGE and assayed for urease specific activity.

Urease apoprotein was purified from cells containing the pKK17 plasmid as described previously.[8]

RESULTS

Creation of a *Ka*UreD Homology Model and Targeting Residues To Substitute. To investigate the function of *Ka*UreD in the maturation of *K. aerogenes* urease, we examined a series of *ureD* mutants for their effects on urease activity, metal content, and UreD/urease and UreD/UreF protein−protein interactions. Residues targeted for substitution were based, in part, on a multiple sequence alignment of 32 homologous sequences that identified the conserved residues in UreD/UreH proteins (Figure S1). Note that *Hp*UreH is the only one of these proteins for which a crystal structure is known and that *Ka*UreD is the only other representative that has been biochemically characterized. No metal-binding motifs were apparent within the alignment, nor were any metal-binding motifs identified for *Hp*UreH within the *Hp*UreH/UreF/UreG structure.[31]

To guide substitution of surface residues that may facilitate protein−protein interactions or participate in a hand-off mechanism of nickel transfer, we prepared a *Ka*UreD homology model with the crystal structure of *Hp*UreH in the *Hp*UreH/UreF/UreG complex[31] serving as the template (Figure 1A) and refined the model by MD simulations. Sequence conservation mapped onto the homology model revealed a region of highly conserved, surface-exposed residues on the face opposite to that of the UreF binding site (Figure 1C). This region could function as the UreD/urease binding interface. Conserved surface residues in this region of the protein (Y42, E46, C48, H49, H54, D63, K86, Y88, R89, R148, and E153) were substituted. In addition, a few surface residues on the reverse face or near the *Ka*UreD/UreF interface (R163, E165, D169, E176, T196, and R211) were chosen for substitution.

Additional residues selected for substitution were predicted to be at least partially buried in the protein and may be

DOI: 10.1021/acs.biochem.5b00942
Biochemistry 2015, 54, 6392−6401

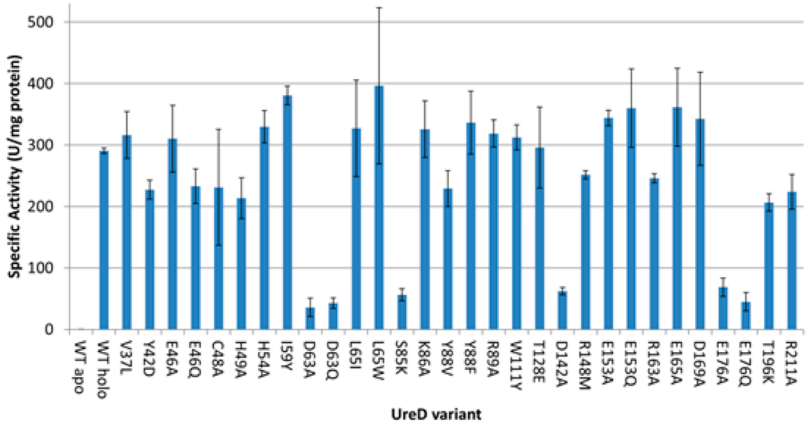

Figure 2. Urease activities of cell-free extracts from cells containing *Ka*UreD variants. *E. coli* BL21(DE3) cells were transformed with plasmid pKK17D* (encoding *ureD*ABCEFG*), grown in LB containing 1 mM $NiCl_2$ (except for the sample producing urease apoprotein, which was not supplemented with the metal), and soluble cell-free extracts were assayed for urease activity. Error bars represent triplicate analyses of biological replicates (n = 3 in all cases except R163A and T196K samples, where n = 2).

important for urease activation if the tunnel hypothesis is correct. Channels within *Hp*UreH/UreF/UreG[26] had been predicted by using CAVER;[51] we identified similar channels in the same complex (Figure S2) based on the average structure from 150 ns MD using MOLE.[46] When these procedures were applied to the refined *Ka*UreD model, a set of tunnels was predicted to branch from a common entry site near E176, at the likely *Ka*UreD/UreF interface, and exit through any of four pathways (Figure 1B). The origin of these tunnels is unchanged from the internal channel predicted for *Hp*UreH, and tunnel 1 of the *Ka*UreD homology model is similar to the tunnel predicted in *Hp*UreH/UreF/UreG. However, the three novel exits in the *Ka*UreD model (tunnels 2, 3, and 4 in Figure 1B) were not predicted by either CAVER or MOLE analysis of the *Hp*UreH/UreF/UreG structure. To test the importance of the four channels in urease activation, nonsurface (internal) residues were changed. For example, E176 in *Ka*UreD, analogous to *Hp*UreH D174 located at the *Hp*UreH/UreF interface, was substituted with similarly sized or smaller residues, in both cases lacking a negative charge. Several additional substitutions were designed to place bulky (F, Y, or W) or lengthy (K or E) residues at positions within or at the termini of the tunnels (e.g., V37, I59, D63, L65, S85, W111, T128, and T196). For each alteration, the substitute residue was modeled into *Ka*UreD using PyMOL and analyzed to ensure that most rotamers did not have steric clashes. Models containing potential tunnel-blocking changes were analyzed by MOLE to assess whether the substitutions exhibited the desired effect of eliminating the tunnel. Variants that blocked the water tunnels *in silico* were selected for experimental study. The selected residues and the corresponding *H. pylori* residue numbers are illustrated in Figure 1B,C. The set of substitutions, primers utilized, rationale for the mutations, and conservation scores of the residues are listed in Table S1.

Effects of *Ka*UreD Variants on the *in Vivo* Activity of Urease. To determine whether the mutations summarized above affected *in vivo* urease maturation, we cultured cells containing pKK17D* (the asterisk indicates *ureD* mutations) in LB in the presence of 1 mM Ni^{2+}. SDS-PAGE was used to confirm that equivalent levels of urease protein were produced in all cultures. Substitutions of surface-exposed residues in the *Ka*UreD model did not appreciably alter the urease activities when assayed using soluble cell-free extracts (Figure 2). In contrast, significantly reduced levels (<30%) of *in vivo* urease activity relative to that of cells containing WT *Ka*UreD were noted for cells producing six other variants with substitutions surrounding a predicted 34.6 Å tunnel (Figure 1B). Cellular activation of urease using E176A or E176Q variants of *Ka*UreD resulted in activities that were 24% and 16% of those with WT *Ka*UreD. E176 of *Ka*UreD corresponds to D174 in the *H. pylori* protein, located at the *Hp*UreH/UreF interfacial site but not directly involved in bonding. The D142A variant of *Ka*UreD led to 21% of WT urease activity. This residue (corresponding to E140 in *Hp*UreH) is predicted to be buried, forming backbone-mediated contacts with the side chain of T196 and a hydrogen bond between its carboxylate and the backbone carbonyl of L143. Since β-sheet formation and stability is dominated by backbone hydrogen bonding, loss of the polar interaction is unlikely to affect the overall structural stability of *Ka*UreD. S85 is positioned with its side chain facing the shared branch point for the tunnels. The S85K variant yielded cell-free extract urease activities that were 19% relative to those for WT *Ka*UreD. D63 resides on the face of *Ka*UreD lying opposite the likely UreF interface and is positioned at the exit point of the 34.6 Å tunnel. Changing this residue (to A or Q) resulted in cell-free extracts with 12% and 15% of WT urease activities. Surprisingly, T196K *Ka*UreD, containing a substitution designed to block the entrance point of the tunnel at the *Ka*UreD/UreF interface, had only a mild effect on urease maturation (i.e., 71% of WT activity); however, the predicted effects were based on a static homology model so the outcome in a dynamic structure cannot be assured. In sum, these results support the existence of a channel within *Ka*UreD that is important for urease activation, but they do not establish the function of the tunnel.

Pull-Down Assays. To identify whether urease/UreD or UreD/UreF protein−protein interactions were disrupted for the six *Ka*UreD variants deficient in urease activation, we substituted the corresponding *ureD* sequences into pKKG (the urease gene cluster encoding *Ka*UreG with a C-terminal *Strep*-II tag),[11] cultured the *E. coli* pKKGD* cells in LB that lacked Ni^{2+}, and examined the resulting urease/UreD/UreF/$UreG_{Str}$ complexes after *Strep*-Tactin enrichment. Constructs encoding WT and R211A *Ka*UreD (providing 77% activity relative to WT) were used as controls (with replicate analysis of the WT sample yielding more intense bands for the accessory proteins).

DOI: 10.1021/acs.biochem.5b00942
Biochemistry 2015, 54, 6392−6401

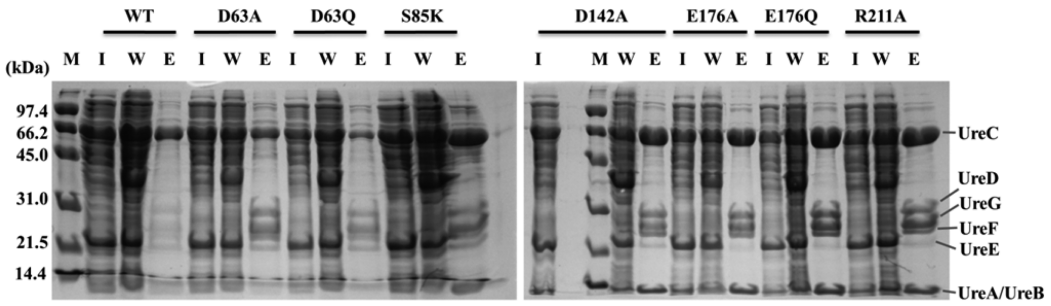

Figure 3. Interactions of *Ka*UreG$_{Str}$ with other urease proteins. *E. coli* BL21(DE3) cells were transformed with pKKD*G producing the *Ka*UreD variants noted above the lanes. Soluble cell-free extracts (I, for input) were chromatographed on *Strep*-Tactin resin with the unbound wash (W) and the desthiobiotin-eluted (E) fractions analyzed by SDS-PAGE.

In all cases, the cell-free extracts contained similar levels of urease, and the UreG$_{Str}$ fractions eluted from the *Strep*-Tactin resin contained the urease subunits, UreD, UreF, and UreG accessory proteins (Figure 3). These results demonstrated that urease/*Ka*UreD and *Ka*UreD/UreF interactions were maintained when using the *Ka*UreD variants, and they suggest that variant *Ka*UreD proteins were properly folded.

Analysis of the Activities and Metal Contents of Urease Samples Activated by Variant *Ka*UreDs. To examine whether *ureD* mutant cultures with reduced urease activities produced enzyme that was altered in metal content, we enriched urease samples from selected *E. coli* pKKD*G cells cultured in the presence of 1 mM Ni^{2+} (LB binds nickel with great affinity, thus limiting urease activation efficiency) and analyzed the enzyme specific activities and metal contents. The urease samples were enriched to >90% purity (Figure S3), and their specific activities (Table 2) generally paralleled those measured in cell-free extracts where urease comprised approximately 15% of the cellular protein (Figure 2). While the *Ka*UreD variants giving rise to reduced activity in the cell-free extracts also exhibited reduced specific activities for the enriched proteins, detailed comparisons of the results underscore differences. For example, urease activity in cell-free extracts produced by D63A *Ka*UreD exhibited only 12% of the WT activity, whereas the purified urease from this sample exhibited 26% of the WT enzyme activity. The samples associated with E176A *Ka*UreD also yielded greater activity for the purified enzyme than expected from the cell-free extracts. In contrast, the purified urease specific activities were lower than expected on the basis of cell-free urease activities for the samples associated with D63Q and D142A *Ka*UreD. Inspection of the metal contents for the enriched ureases with low urease specific activity revealed less nickel than those activated with WT *Ka*UreD and identified varying levels of zinc and iron (Table 2), with the greatest levels of zinc corresponding to the most inactive urease, generated with D142A *Ka*UreD. These findings confirm that tunnel-blocking variants of *Ka*UreD lead to deficiencies in urease nickel content, consistent with a nickel-transfer role for the channel.

Table 2. Specific Activities and Metal Contents of Urease Samples Enriched from Cells Containing Selected *Ka*UreD Variants[a]

*Ka*UreD variant	specific activity, U/(mg protein) (% WT)	Ni per UreABC (% WT)	Zn per UreABC	Fe per UreABC
WT(−Ni) pKK17D	0	0.004 (4×10^{-5})	0.13	0.27
WT pKKDG	1690 (100)	1.1 (100)	0	0.02
D63A pKKDG	434 (25.7)	0.54 (49.1)	0.16	0.21
D63Q pKKDG	55.7 (3.29)	0.22 (20.0)	0.34	0.07
S85K pKKDG	487 (28.8)	0.39 (35.5)	0.06	0.30
D142A pKKDG	14.1 (0.84)	0.07 (6.4)	0.52	0.14
E176A pKKDG	1080 (63.7)	0.51 (46.4)	0.09	0.11
E176Q pKKDG	375 (22.2)	0.43 (39.1)	0.03	0.13
R211A pKKDG	1230 (72.4)	0.76 (69.1)	0.21	0.29

[a]The urease samples were enriched from cell-free extracts of *E. coli* pKKD*G grown in LB containing 1 mM $NiCl_2$, except for a sample of urease apoprotein that was obtained from *E. coli* pKK17D grown in LB lacking nickel (−Ni). Units of urease activity are μmol min^{-1} (mg protein)$^{-1}$. Metal contents were determined by inductively coupled plasma atomic emission spectroscopy.

MD of Activation-Deficient *Ka*UreD Constructs. To analyze the effects of the *Ka*UreD variants on the overall stabilities of the predicted tunnels, MD simulations were carried out on the refined *Ka*UreD model and ten variants. These included the six substituted proteins that resulted in a loss of function (D63A/Q, S85K, E142A, and E176A/Q) along with four variants (L65I/W, T128E, and T196K) that were initially predicted to block the tunnel but did not result in a loss of function. Root mean square deviations (RMSDs) of all heavy atoms for the variant systems were similar to WT, suggesting that the substitutions did not induce large conformational changes (Figure S4). *Ka*UreD alone exhibited only slightly more flexibility (by about 0.5 Å RMSD) than either *Hp*UreH protomer in (*Hp*UreH/UreF/UreG)$_2$, suggesting that separating *Ka*UreD from the complex does not have a large effect on its conformation.

To analyze the effects of substituting side chains along the proposed channels and other possible channels, clustering analysis was applied to the combined conformations of the last 30 ns trajectories of all 11 *Ka*UreD systems. All the sampled structures were grouped into eight clusters (C1−C8). The conformations with the smallest RMSD to the cluster centers were used as representative structures to probe the channels originating at E176 by MOLE (Figure 4 and Table S2). The largest cluster (C1), dominant in the WT and T196K models of *Ka*UreD (green in Figure 4), possessed a channel capable of accommodating 6-coordinate Ni^{2+} with a radius of 0.69−0.715 Å.[52] This channel is almost the same as the proposed channel. Other channels wide enough to allow Ni^{2+} to pass were also

DOI: 10.1021/acs.biochem.5b00942
Biochemistry 2015, 54, 6392−6401

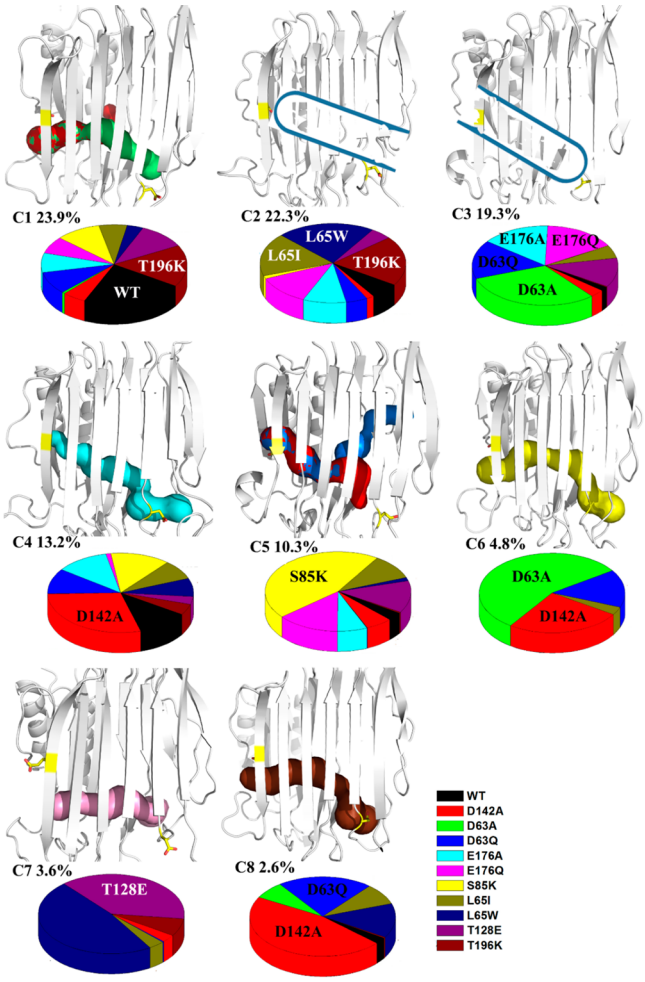

Figure 4. Channels associated with the eight main clustered conformations derived from MD simulations, with the constitutions of the corresponding clusters shown below in pie charts. All channels leading from the position around E176 (traversing *Ka*UreD from left to right) are shown with different colors. E176 and D63 are shown as yellow sticks. Clusters C2 and C3 possess blocked channels at one or the other end, with the cavities depicted in blue outline.

found in the smaller C6 and C7 clusters in the D63A/D142A and L65W/T128E *Ka*UreD variants. All of these available channels have an ending/entrance located near D63. In other structures, viable channels leading from E176 were not identified because there was either a narrow bottleneck along the path (red channel in Figure 4 for C1 and channels in C4, C5, and C8), or the E176 (C2) or D63 (C3) ends were blocked (blue outlines in Figure 4) so that Ni^{2+} passage would be considered unlikely. The blocked channels in C2 and C3 resulted from side chain dynamics, but this freedom of rotation might be occluded by *Ka*UreD/UreF or *Ka*UreD/urease interactions, as evidenced by the lower RMSD observed for the *Hp*UreD/UreF protein−protein complex (Figure S4). Therefore, the cavity in C2 based on the *Ka*UreD L65I/L65W/T196K models may not be representative of what would be observed in the *Ka*UreD/UreF/UreG complex. All the eight representative structures were submitted to electrostatics calculations (Figure S5). The exit located near D63 with a negative electrostatic potential in cluster C1 turned into a positive electrostatic potential in other clusters. To conclude, the clustering analysis results revealed that all the systems have multiple dynamic channels initiating at the interface with UreF and ending near D63, providing a possible explanation for the remaining low urease activity levels in the variants.

DISCUSSION

It has been estimated that about 1/3 of all proteins contain metals, with ∼40% of metalloproteins having metal centers essential for catalysis.[53,54] These proteins must overcome several challenges during their synthesis in order to incorporate the proper metal(s) to become functional. One approach to circumvent mismetalation is to use accessory proteins for binding the metal, synthesizing any metallocofactor shown to be present, and transferring it into the nascent metalloenzyme active sites.[54−56] Examples of this strategy are seen in the Nif proteins involved in biosynthesis of the FeMoco cofactor of nitrogenase,[57] the Hyp proteins used to generate the [NiFe]-hydrogenase cofactor,[58] the copper chaperone for superoxide dismutase required for Cu,Zn-superoxide dismutase,[59] and, the focus here, the maturation of nickel-containing urease.[5]

Role of *Ka*UreD in Urease Activation. *Ka*UreD is required for *in vivo* maturation of *K. aerogenes* urease, it forms a complex with the apoenzyme, and it interacts with *Ka*UreF and *Ka*UreG, the latter of which accepts nickel from *Ka*UreE.[5] Two potential roles in transferring nickel have been posited for UreD/UreH homologues, beyond the structural role of connecting UreE and the urease apoprotein. One hypothesis suggests that *Ka*UreD surface residues function in a "bucket brigade" approach to shuttle the nickel from its delivery site on *Ka*UreG to the nascent active site.[8,11] Precedence for such a hand-off mechanism includes Cox17 and ScoI, which pass Cu^{1+} into cytochrome *c* oxidase.[60] An alternative hypothesis with no direct precedent is derived from the *Hp*UreH/UreF/UreG crystal structure[31] for which a buried water tunnel was predicted to span from the likely nickel-binding site in *Hp*UreG through *Hp*UreF and *Hp*UreH, potentially functioning to deliver nickel for urease maturation.[26] Significantly, no direct experimental support for a nickel transfer tunnel was reported. The studies described here provide compelling evidence that a buried channel in *Ka*UreD is used to deliver nickel to urease apoprotein rather than transferring the metal ion via surface residues.

We characterized the effects on urease activity for 30 variant forms of *Ka*UreD that were designed to disrupt potential surface metal-transfer sites and internal channels. None of the *Ka*UreD surface substitutions led to significant losses of urease activity in cell-free extracts, implying that the surface residues examined are not of great importance to the function of *Ka*UreD. In sharp contrast, *Ka*UreD variants with alterations at the ends (E176A/Q and D63A/Q) and the initial branch point (D142A) of predicted tunnel 1 exhibit significant losses in urease activity. The S85K *Ka*UreD variant, designed to block the shared branch point, also led to decreased urease activity. MD simulations reveal that these substitutions either narrow the channel or block an exit. One *Ka*UreD variant designed to block the exit of tunnel 1 (I59Y) had no appreciable effect on urease activity; however, this residue is located on a disordered loop in the model and likely adopts multiple conformations that would not be accurately depicted using analysis of a static structure. T196K *Ka*UreD had no appreciable effect on urease activation *in vivo*, even though *in silico* analysis of the available rotamers predicted blockage of the tunnel entrance and the introduction of a positive charge (as in the S85K variant) could reasonably increase the energy barrier of Ni^{2+} transport. MD

DOI: 10.1021/acs.biochem.5b00942
Biochemistry 2015, 54, 6392−6401

simulations suggest the tunnel of this variant exists largely in WT conformation, explaining this lack of effect. Unfortunately, no modifications to residues facing tunnel 2 could be modeled to block the tunnel without encountering severe steric clashes, but the lack of this tunnel in *Hp*UreH and the clear tunnel 1-disrupting effects reduce the probability that this channel has a role. Overall, MD simulations support the existence of multiple dynamic channels (Figure 4), so that blocking one channel may be insufficient to abolish UreD function because new channels could form due to side chain dynamics. In sum, the MD and cell-free extract activity results are consistent with a tunnel within *Ka*UreD functioning in urease activation, but loss of urease activity also could arise from disruption of protein−protein interactions.

*Ka*UreD variants of interest were shown to be capable of interacting with their known binding partners according to pull-down studies carried out using nickel-free cells containing pKKD*G. The WT construct activates urease comparable to nontagged *Ka*UreG,[11] and *Strep*-Tactin enrichments contain *Ka*UreG$_{Str}$ along with the urease subunits, *Ka*UreD and *Ka*UreF. This result shows that protein−protein binding interactions are not disrupted when using the selected *Ka*UreD variants and provides evidence for their proper folding. This finding is especially important in the case of the S85K variant, where the introduction of a positive charge buried within the protein was a point of concern.

The decreased urease activities in cells producing *Ka*UreD variants correlate with lower nickel contents of the corresponding ureases. Of interest, urease samples that were deficient in activity and nickel content, including the urease apoprotein control, possess contaminating levels of zinc and iron. Most notably, ureases activated with the D63Q and D142A *Ka*UreD variants exhibit the lowest urease activities and nickel contents as well as the highest zinc occupancies. These results are compatible with the selected variants disrupting a nickel transfer tunnel, leading to spurious metal incorporation (zinc and iron) into urease. The mechanism of mismetalation may occur via metal binding to the free urease apoprotein, which seems unlikely given the stability of *Ka*UreABC/UreD/UreF/UreG during purification, or by binding to apoprotein within the complex, requiring a secondary metal access route that may inefficiently and opportunistically incorporate divalent metal ions when the nickel transfer tunnel is blocked. Upon apoprotein metalation, the complex dissociates to release the metal-substituted enzyme. The function of the other accessory proteins are presumably unaltered in cells containing the variant *Ka*UreD proteins, so acquisition of nickel by *Ka*UreE, transfer to *Ka*UreG, and passage through *Ka*UreF should remain unaffected. For WT cells with Ni^{2+} present, the mismetalation pathway is outcompeted by the GTP-dependent process that loads the correct metal into the nickel-transfer tunnel starting in UreF. The GTP dependence of nickel loading may provide the driving force so that nickel incorporation into urease apoprotein is not simply diffusion controlled.

Comparison of the *Ka*UreD Internal Channel to Other Protein Tunnels. We have shown that *Ka*UreD possesses a tunnel required for nickel delivery to the cognate urease. The residues lining this tunnel, shown in Figure 5, lack positive charges that could impose a high thermodynamic penalty for cation movement. Negatively charged residues (D63, D142, and E176) are localized near the tunnel ends. The diameter of the tunnel, ranging from 1.2 to 2.5 Å, can accommodate Ni^{2+} with a radius of 0.69−0.715 Å,[52] especially when considering

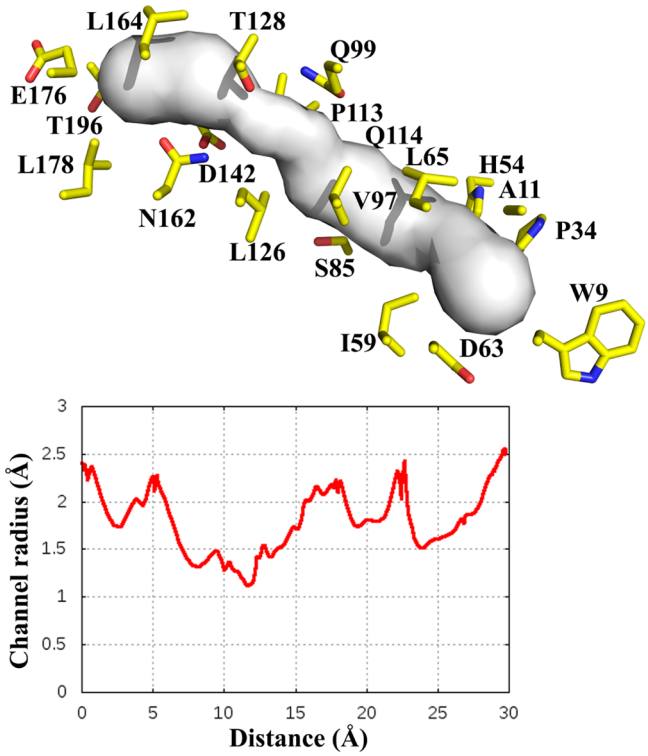

Figure 5. Characteristics of the main *Ka*UreD internal channel. The main channel probed in WT *Ka*UreD is shown in the upper panel in white with the *Ka*UreF binding site to the left and the exit to the right. Residues lining the channel are shown in stick mode. The radius of the channel as a function of distance from the tunnel entrance is shown in the bottom panel.

the protein dynamics. The conclusion that *Ka*UreD has a nickel-transfer tunnel fits well with results from nickel-binding studies of UreABC/*Ka*UreD and MBP−*Ka*UreD, as well as the computation-based proposal of a functional tunnel in *Hp*UreH/UreF/UreG.[8,16,26] Our data do not address the additional possibility that the tunnel also may be utilized for delivery of CO_2 for carbamylating the lysine to form a bridging ligand of the dinuclear metallocenter.

Internal channels are known to serve important roles in other proteins, including the molecular tunnels used to prevent diffusion of toxic or short-lived intermediates in a variety of enzymes.[61] Few precedents exist, however, for metal transfer tunnels. The cation transport proteins are designed for energy-driven, unidirectional transport across cell membranes,[62] but the tunnels are not continuously open to prevent energy dissipation. A tunnel strategy is used for iron transfer into the ferritin core,[63] but this process involves metal storage rather than metalloenzyme activation. The Fe−Fe hydrogenase HydA includes a cationic channel that allows for insertion of a 2Fe subcluster during metallocenter biosynthesis,[64] but this partial tunnel is located within the enzyme itself rather than in an accessory protein. *Ka*UreD thus serves as a new paradigm for metallocenter assembly using an internal metal transfer process.

■ ASSOCIATED CONTENT

Ⓢ Supporting Information

The Supporting Information is available free of charge on the ACS Publications website at DOI: 10.1021/acs.biochem.5b00942.

DOI: 10.1021/acs.biochem.5b00942
Biochemistry 2015, 54, 6392−6401

Primers, rationale, and conservation score for *Ka*UreD variants, contributions of the clusters to each KaUreD system, multiple sequence alignment of UreD homologs used in Consurf conservation analysis, channels predicted in the $(HpUreH/UreF/UreG)_2$ complex by MOLE 2.0, enriched urease samples that were activated in vivo using *Ka*UreD variants, stability of WT and selected variants of *Ka*UreD and *Hp*UreH, and electrostatic surface potentials for representative structures of the eight clusters (PDF)

AUTHOR INFORMATION

Corresponding Author

*Mailing address: Department of Microbiology and Molecular Genetics, 567 Wilson Road, room 2215, Biomedical Physical Sciences, Michigan State University, East Lansing, MI 48824-4320. Phone: 517-884-5404. E-mail: hausinge@msu.edu.

Funding

This work was supported in part by the National Institutes of Health (Grant DK04586 to R.P.H.) and Michigan State University Dissertation Continuation and Completion Fellowships (to M.A.F.).

Notes

The authors declare no competing financial interest.

ACKNOWLEDGMENTS

We thank Eric Carter for initiating residue substitution studies of MBP−UreD.

ABBREVIATIONS

HEPES, 4-(2-hydroxyethyl)-1-piperazineethanesulfonic acid; IPTG, isopropyl β-D-1-thiogalactopyranoside; LB, lysogeny broth; MBP, maltose binding protein; MD, molecular dynamics; SDS-PAGE, sodium dodecyl sulfate−polyacrylamide gel electrophoresis; WT, wild-type

REFERENCES

(1) Zambelli, B., Musiani, F., Benini, S., and Ciurli, S. (2011) Chemistry of Ni^{2+} in urease: Sensing, trafficking, and catalysis. *Acc. Chem. Res. 44*, 520−530.

(2) Krajewska, B. (2009) Ureases I. Functional, catalytic and kinetic properties: A review. *J. Mol. Catal. B: Enzym. 59*, 9−21.

(3) Witte, C.-P. (2011) Urea metabolism in plants. *Plant Sci. 180*, 431−438.

(4) Mobley, H. L. T., and Hausinger, R. P. (1989) Microbial ureases: Significance, regulation, and molecular characterization. *Microbiol. Rev. 53*, 85−108.

(5) Farrugia, M. A., Macomber, L., and Hausinger, R. P. (2013) Biosynthesis of the urease metallocenter. *J. Biol. Chem. 288*, 13178−13185.

(6) Lee, M. H., Mulrooney, S. B., Renner, M. J., Markowicz, Y., and Hausinger, R. P. (1992) *Klebsiella aerogenes* urease gene cluster: Sequence of *ureD* and demonstration that four accessory genes (*ureD*, *ureE*, *ureF*, and *ureG*) are involved in nickel metallocenter biosynthesis. *J. Bacteriol. 174*, 4324−4330.

(7) Jabri, E., Carr, M. B., Hausinger, R. P., and Karplus, P. A. (1995) The crystal structure of urease from *Klebsiella aerogenes*. *Science 268*, 998−1004.

(8) Carter, E. L., and Hausinger, R. P. (2010) Characterization of *Klebsiella aerogenes* urease accessory protein UreD in fusion with the maltose binding protein. *J. Bacteriol. 192*, 2294−2304.

(9) Boer, J. L., and Hausinger, R. P. (2012) *Klebsiella aerogenes* UreF: Identification of the UreG binding site and role in enhancing the fidelity of urease activation. *Biochemistry 51*, 2298−2308.

(10) Moncrief, M. B. C., and Hausinger, R. P. (1997) Characterization of UreG, identification of a UreD-UreF-UreG complex, and evidence suggesting that a nucleotide-binding site in UreG is required for *in vivo* metallocenter assembly of *Klebsiella aerogenes* urease. *J. Bacteriol. 179*, 4081−4086.

(11) Boer, J. L., Quiroz-Valenzuela, S., Anderson, K. L., and Hausinger, R. P. (2010) Mutagenesis of *Klebsiella aerogenes* UreG to probe nickel binding and interactions with other urease-related proteins. *Biochemistry 49*, 5859−5869.

(12) Song, H. K., Mulrooney, S. B., Huber, R., and Hausinger, R. P. (2001) Crystal structure of *Klebsiella aerogenes* UreE, a nickel-binding metallochaperone for urease activation. *J. Biol. Chem. 276*, 49359−49364.

(13) Colpas, G. J., Brayman, T. G., Ming, L.-J., and Hausinger, R. P. (1999) Identification of metal-binding residues in the *Klebsiella aerogenes* urease nickel metallochaperone, UreE. *Biochemistry 38*, 4078−4088.

(14) Mulrooney, S. B., and Hausinger, R. P. (1990) Sequence of the *Klebsiella aerogenes* urease genes and evidence for accessory proteins facilitating nickel incorporation. *J. Bacteriol. 172*, 5837−5843.

(15) Park, I.-S., and Hausinger, R. P. (1995) Requirement of carbon dioxide for *in vitro* assembly of the urease nickel metallocenter. *Science 267*, 1156−1158.

(16) Park, I.-S., and Hausinger, R. P. (1996) Metal ion interactions with urease and UreD-urease apoproteins. *Biochemistry 35*, 5345−5352.

(17) Park, I.-S., Carr, M. B., and Hausinger, R. P. (1994) *In vitro* activation of urease apoprotein and role of UreD as a chaperone required for nickel metallocenter assembly. *Proc. Natl. Acad. Sci. U. S. A. 91*, 3233−3237.

(18) Quiroz-Valenzuela, S., Sukuru, S. C. K., Hausinger, R. P., Kuhn, L. A., and Heller, W. T. (2008) The structure of urease activation complexes examined by flexibility analysis, mutagenesis, and small-angle X-ray scattering. *Arch. Biochem. Biophys. 480*, 51−57.

(19) Chang, Z., Kuchar, J., and Hausinger, R. P. (2004) Chemical crosslinking and mass spectrometric identification of sites of interaction for UreD, UreF, and urease. *J. Biol. Chem. 279*, 15305−15313.

(20) Moncrief, M. B. C., and Hausinger, R. P. (1996) Purification and activation properties of UreD-UreF-urease apoprotein complexes. *J. Bacteriol. 178*, 5417−5421.

(21) Soriano, A., and Hausinger, R. P. (1999) GTP-dependent activation of urease apoprotein in complex with the UreD, UreF, and UreG accessory proteins. *Proc. Natl. Acad. Sci. U. S. A. 96*, 11140−11144.

(22) Farrugia, M. A., Han, L., Zhong, Y., Boer, J. L., Ruotolo, B. T., and Hausinger, R. P. (2013) Analysis of a soluble $(UreD:UreF:UreG)_2$ accessory protein complex and its interactions with *Klebsiella aerogenes* urease by mass spectroscopy. *J. Am. Soc. Mass Spectrom. 24*, 1328−1337.

(23) Cussac, V., Ferrero, R. L., and Labigne, A. (1992) Expression of *Helicobacter pylori* urease genes in *Escherichia coli* grown under nitrogen-limiting conditions. *J. Bacteriol. 174*, 2466−2473.

(24) Ha, N.-C., Oh, S.-T., Sung, J. Y., Cha, K. A., Lee, M. H., and Oh, B.-H. (2001) Supramolecular assembly and acid resistance of *Helicobacter pylori* urease. *Nat. Struct. Biol. 8*, 505−509.

(25) Lam, R., Romanov, V., Johns, K., Battaile, K., Wu-Brown, J., Guthrie, J. L., Hausinger, R. P., Pai, E., and Chirgadze, N. Y. (2010) Crystal structure of a truncated urease accessory protein UreF from *Helicobacter pylori*. *Proteins: Struct., Funct., Genet. 78*, 2839−2848.

(26) Zambelli, B., Berardi, A., Martin-Diaconescu, V., Mazzei, L., Musiani, F., Maroney, M. J., and Ciurli, S. (2014) Nickel binding properties of *Helicobacter pylori* UreF, an accessory protein in the nickel-based activation of urease. *JBIC, J. Biol. Inorg. Chem. 19*, 319−334.

(27) Bellucci, M., Zambelli, B., Musiani, F., Turano, P., and Ciurli, S. (2009) *Helicobacter pylori* UreE, a urease accessory protein: Specific Ni^{2+}- and Zn^{2+}-binding properties and interaction with its cognate UreG. *Biochem. J. 422*, 91−100.

DOI: 10.1021/acs.biochem.5b00942
Biochemistry 2015, 54, 6392−6401

(28) Shi, R., Munger, C., Asinas, A., Benoit, S. L., Miller, E., Matte, A., Maier, R. J., and Cygler, M. (2010) Crystal structures of apo and metal-bound forms of the UreE protein from *Helicobacter pylori*: Role of multiple metal binding sites. *Biochemistry 49*, 7080−7088.
(29) Yang, X., Li, H., Lai, T.-P., and Sun, H. (2015) UreE-UreG complex facilitates nickel transfer and preactivates GTPase of UreG in *Helicobacter pylori*. *J. Biol. Chem. 290*, 12474−12485.
(30) Strugatsky, D., McNulty, R., Munson, K., Chen, C.-K., Soltis, S. M., Sachs, G., and Luecke, H. (2012) Structure of the proton-gated urea channel from the gastric pathogen *Helicobacter pylori*. *Nature 493*, 255−258.
(31) Fong, Y. H., Wong, H. C., Yuen, M. H., Lau, P. H., Chen, Y. W., and Wong, K.-B. (2013) Structure of UreG/UreF/UreH complex reveals how urease accessory proteins facilitate maturation of *Helicobacter pylori* urease. *PLoS Biol. 11*, e1001678.
(32) Kelley, L. A., and Sternberg, M. J. (2009) Protein structure prediction on the web: A case study using Phyre server. *Nat. Protoc. 4*, 363−371.
(33) Johnson, M. K., Zaretskaya, I., Raytselis, Y., Merezhuk, Y., McGinnis, S., and Madden, T. L. (2008) NCBI BLAST: A better web interface. *Nucleic Acids Res. 36*, W5−W9.
(34) McWilliam, H., Li, W., Uludag, M., Squizzato, S., Park, Y. M., Buso, N., Cowley, A. P., and Lopez, R. (2013) Analysis tool web services from the EMBL-EBI. *Nucleic Acids Res. 41*, W597−W600.
(35) Celniker, G., Nimrod, G., Ashkenazy, H., Glaser, F., Martz, E., Mayrose, I., Pupko, T., and Ben-Tal, N. (2013) ConSurf: Using evolutionary data to raise testable hypotheses about protein function. *Isr. J. Chem. 53*, 199−206.
(36) Mirjalili, V., and Feig, M. (2013) Protein structure refinement through structure selection and averaging from molecular dynamics ensembles. *J. Chem. Theory Comput. 9*, 1294−1303.
(37) Humphrey, W., Dalke, A., and Schulten, K. (1996) VMD: Visual molecular dynamics. *J. Mol. Graphics 14*, 33−38.
(38) van Eunen, K., Bouwman, J., Westerhoff, H. V., Bakker, B. M., et al. (2010) Measuring enzyme activities under standardized in vivo-like conditions for systems biology. *FEBS J. 277*, 749−760.
(39) Phillips, J. C., Braun, R., Wang, W.-J., Gumbart, J., Tajkhorshid, E., Villa, E., Chipot, C., Skeel, R. D., et al. (2005) Scalable molecular dynamics with NAMD. *J. Comput. Chem. 26*, 1781−1802.
(40) MacKerell, A. D., Feig, M., and Brooks, C. L. (2004) Improved treatment of the protein backbone in empirical force fields. *J. Am. Chem. Soc. 126*, 698−699.
(41) Best, R. B., Zhu, X., Shim, J., Lopes, P. E. M., Mittal, J., Feig, M., and MacKerell, A. D. (2012) Optimization of the additive CHARMM all-atom protein force field targeting improved sampling of the backbone Φ, ψ, and side-chain $\chi(1)$ and $\chi(2)$ dihedral angles. *J. Chem. Theory Comput. 8*, 3257−3273.
(42) Darden, T., York, D., and Pedersen, L. (1993) Particle mesh Ewald: An $N\cdot\log(N)$ method for Ewald sums in large systems. *J. Chem. Phys. 98*, 10089−10092.
(43) Miyamoto, S., and Kollman, P. A. (1992) Settle: An analytical version of the shake and rattle algorithm for rigid water model. *J. Comput. Chem. 13*, 952−962.
(44) Martyna, G. J., Tobias, D. J., and Klein, M. L. (1994) Constant-pressure molecular dynamics algorithms. *J. Chem. Phys. 101*, 4177−4189.
(45) Feller, S. E., Zhang, Y. H., Pastor, R. W., and Brooks, C. L. (1995) Constant pressure molecular dynamics simulation: The Langevin piston method. *J. Chem. Phys. 103*, 4613−4621.
(46) Sehnal, D., Varekovaa, R. S., Berka, K., Pravda, L., Navratilova, V., Banas, P., Ionescu, C. M., Otyepka, M., and Koca, J. (2013) MOLE 2.0: Advanced approach for analysis of biomacromolecular channels. *J. Cheminf. 5*, 39.
(47) Baker, N. A., Sept, D., Joseph, S., Holst, M. J., and McCammon, J. A. (2001) Electrostatics of nanosystems: application to microtubules and the ribosome. *Proc. Natl. Acad. Sci. U. S. A. 98*, 10037−10041.
(48) Feig, M., Karanicolas, J., and Brooks, C. L., III. (2004) MMTSB tool set: Enhanced sampling and multiscale modeling methods for applications in structural biology. *J. Mol. Graphics Modell. 22*, 377−395.
(49) The PyMOL Molecular Graphics System, Version 1.7.4 ed., Schrödinger, LCC.
(50) Weatherburn, M. W. (1967) Phenol-hypochlorite reaction for determination of ammonia. *Anal. Chem. 39*, 971−974.
(51) Chovancova, E., Pavelka, A., Benes, P., Strnad, O., Brezovsky, J., Koszlikova, B., Gora, A., Sustr, V., Klvana, M., Medek, P., Biedermannova, L., Sochor, J., and Damborsky, J. (2012) CAVER 3.0: A tool for the analysis of transport pathways in dynamic protein structures. *PLoS Comput. Biol. 8*, e1002708.
(52) Persson, I. (2010) Hydrated metal ions in aqueous solution: How regular are their structures. *Pure Appl. Chem. 82*, 1901−1917.
(53) Andreini, C., Bertini, I., Cavallaro, G., Holliday, G. L., and Thornton, J. M. (2008) Metal ions in biological catalysis: From enzyme databases to general principles. *JBIC, J. Biol. Inorg. Chem. 13*, 1205−1218.
(54) Waldron, K. J., and Robinson, N. J. (2009) How do bacterial cells ensure that metalloproteins get the correct metal? *Nat. Rev. Microbiol. 7*, 25−35.
(55) Kuchar, J., and Hausinger, R. P. (2004) Biosynthesis of metal sites. *Chem. Rev. 104*, 509−526.
(56) Cotruvo, J. A., Jr., and Stubbe, J. (2012) Metallation and mismetallation of iron and manganese proteins *in vitro* and *in vivo*: the class I ribonucleotide reductases as a case study. *Metallomics 4*, 1020−1036.
(57) Hu, Y., and Ribbe, M. W. (2011) Biosynthesis of nitrogenase FeMoco. *Coord. Chem. Rev. 255*, 1218−1224.
(58) Leach, M. R., and Zamble, D. B. (2007) Metallocenter assembly of the hydrogenase enzymes. *Curr. Opin. Chem. Biol. 11*, 159−165.
(59) Schmidt, P. J., Ramos-Gomez, M., and Culotta, V. C. (1999) A gain of superoxide dismutase (SOD) activity obtained with CSS, the copper metallochaperone for SOD1. *J. Biol. Chem. 274*, 36952−36956.
(60) Robinson, N. J., and Winge, D. R. (2010) Copper metallochaperones. *Annu. Rev. Biochem. 79*, 537−562.
(61) Raushel, F. M., Thoden, J. B., and Holden, H. M. (2003) Enzymes with molecular tunnels. *Acc. Chem. Res. 36*, 539−548.
(62) Maret, W., and Wedd, A., Eds. (2014) *Binding, Transport and Storage of Metal Ions in Biological Cells*, Royal Society of Chemistry, Cambridge, U.K.
(63) Carrondo, M. A. (2003) Ferritins, iron uptake and storage from the bacterioferritin viewpoint. *EMBO J. 22*, 1959−1968.
(64) Mulder, D. W., Boyd, E. S., Sarma, R., Lange, R. K., Endrizzi, J. A., Broderick, J. B., and Peters, J. W. (2010) Stepwise [FeFe]-hydrogenase H-cluster assembly revealed in the structure of $HydA^{\Delta EFG}$. *Nature 465*, 248−251.
(65) Vieira, J., and Messing, J. (1982) The pUC plasmids, an M13mp7-derived system for insertion mutagenesis and sequencing with synthetic universal primers. *Gene 19*, 259−268.
(66) Mulrooney, S. B., Pankratz, H. S., and Hausinger, R. P. (1989) Regulation of gene expression and cellular localization of cloned *Klebsiella aerogenes* (*K. pneumoniae*) urease. *Microbiology 135*, 1769−1776.

DOI: 10.1021/acs.biochem.5b00942
Biochemistry 2015, 54, 6392−6401